

BIOSIGNATURE PRESERVATION AIDED BY ORGANIC-CATION INTERACTIONS IN PROTEROZOIC TIDAL ENVIRONMENTS

KELSEY R. MOORE,¹ THEODORE M. PRESENT,¹ FRANK PAVIA,¹ JOHN P. GROTZINGER,¹ JOSEPH RAZZELL HOLLIS,^{2,3} SUNANDA SHARMA,² DAVID FLANNERY,⁴ TANJA BOSAK,⁵ MICHAEL TUIITE,² ANDREW H. KNOLL,⁶ AND KENNETH WILLIFORD^{2,7}

¹California Institute of Technology, Division of Geological and Planetary Sciences, Pasadena, California 91125, USA

²NASA Jet Propulsion Laboratory, California Institute of Technology, Pasadena, California 91109, USA

³Natural History Museum, London SW7 5BD, UK

⁴Queensland University of Technology School of Earth and Atmospheric Sciences, Brisbane City QLD 4000, Australia

⁵Massachusetts Institute of Technology, Department of Earth, Atmospheric and Planetary Sciences, Cambridge, Massachusetts 02139, USA

⁶Harvard University, Department of Organismic and Evolutionary Biology, Cambridge, Massachusetts 02138, USA

⁷Blue Marble Space Institute of Science, Seattle, Washington, 98104, USA

email: kmoore@caltech.edu

ABSTRACT: The preservation of organic biosignatures during the Proterozoic Eon required specific taphonomic windows that could entomb organic matter to preserve amorphous kerogen and even microbial body fossils before they could be extensively degraded. Some of the best examples of such preservation are found in early diagenetic chert that formed in peritidal environments. This chert contains discrete domains of amorphous kerogen and sometimes kerogenous microbial mat structures and microbial body fossils. Our understanding of how these exquisite microfossils were preserved and the balance between organic degradation and mineral formation has remained incomplete. Here, we present new insights into organic preservation in Proterozoic peritidal environments facilitated through interactions among organic matter, cations, and silica. Organic matter from Proterozoic peritidal environments is not preserved by micro- or cryptocrystalline quartz alone. Rather, preservation includes cation-rich nanoscopic phases containing magnesium, calcium, silica, and aluminum that pre-date chert emplacement and may provide nucleation sites for silica deposition and enable further chert development. Using scanning electron microscopy and elemental mapping with energy dispersive X-ray spectroscopy, we identify cation enrichment in Proterozoic organic matter and cation-rich nanoscopic phases that pre-date chert. We pair these analyses with precipitation experiments to investigate the role of cations in the precipitation of silica from seawater. Our findings suggest that organic preservation in peritidal environments required rapid formation of nanoscopic mineral phases through the interactions of organic matter with seawater. These organic-cation interactions likely laid the initial foundation for the preservation and entombment of biosignatures, paving the way for the development of the fossiliferous chert that now contains these biosignatures and preserves a record of Proterozoic life.

INTRODUCTION

The excellent biosignature preservation potential of Proterozoic marine chert is well established and provides a unique window into the early history of marine microbial life. These chert deposits, interpreted as early diagenetic precipitates, contain kerogen (complex, macromolecular, carbonaceous material) as discrete domains or kerogenous microbial mat textures and even microbial body fossils. In order for kerogen and cellular structures to be preserved, nano- or microcrystalline minerals must have precipitated rapidly from solution around the kerogen before it could be extensively degraded (Knoll and Golubic 1979). However, despite the many studies that have characterized microbial fossils and textures in Proterozoic chert (e.g., Knoll 1985; Schopf and Klein 1992; Knoll et al., 2008; Sergeev and Sharma 2012; Butterfield 2015; Demoulin et al. 2019 and references therein), the chemical mechanism for biosignature preservation in chert remains incompletely understood.

The mechanisms for biosignature preservation via silicification cannot be directly observed or studied in analogous modern marine tidal environments. This is because the ocean today contains only micromolar concentrations of silica (Tréguer et al. 1995) and modern tidal environments

do not precipitate chert. Modern examples of silicification are instead restricted to hot springs and other hydrothermal environments. In these freshwater, hydrothermal systems, silica concentrations can exceed 300 ppm and silica precipitation is an abiotic process in which pure silica polymerizes rapidly from the supersaturated fluid as it cools, encasing any organic matter present (Schultze-Lam et al. 1995; Konhauser et al. 2001; Jones et al. 2004). In these types of environments, if silica concentrations are near amorphous silica saturation (120 ppm at 25°C), pure silica precipitates in the form of friable films that can be dissolved on the timescale of hours to days due to fluctuations in temperature and pH that can re-dissolve the precipitate across solubility boundaries (Wilmeth et al. 2021). In contrast, dense, stable silica that will not be re-dissolved as temperature and pH fluctuate requires silica concentrations of >300 ppm if it precipitates abiotically as a pure silica precipitate (Schultze-Lam et al. 1995; Hinman and Lindstrom 1996; Konhauser et al. 2001; Jones et al. 2004; Orange et al. 2013). The formation of this type of cell-preserving chert from hydrothermal, non-marine systems at supersaturated silica concentrations is quite different from the conditions that characterized Proterozoic marine tidal environments. Therefore, we must seek different models to explain biosignature preservation in Proterozoic tidal environments.

Although Proterozoic marine silica levels were elevated compared to today, with some estimates placing $[\text{SiO}_2]$ between 60 ppm and 120 ppm (Maliva et al. 1989; Siever 1992; Conley et al. 2017; Moore et al. 2020), the preservation of biosignatures in isolated nodules, lenses, and thin beds of chert in otherwise carbonate dominated strata suggests that Proterozoic seawater was not supersaturated with respect to silica everywhere. It has been suggested that evaporative processes in tidal flats helped to increase silica concentrations to a point at which silica could precipitate from solution, supported by the observation that chert in Proterozoic sedimentary successions is almost entirely confined to peritidal environments (Maliva et al. 1989). However, a study that modeled the chemical conditions for Proterozoic chert formation suggested that a range of chemical and biological parameters may be related to chert precipitation alongside evaporative concentration of silica (Manning-Berg and Kah 2017). Moreover, environmental and laboratory studies have shown that the precipitation of abundant, dense, stable silica capable of preserving biosignatures would require silica concentrations well above amorphous silica saturation (Hinman and Lindstrom 1996; Orange et al. 2013; Wilmeth et al. 2021) and polymerization near saturation may be relatively slow (Krauskopf 1956; Chan 1989). Concentrating silica enough to precipitate such abundant, stable chert through evaporation alone would likely take some time, allowing cells and organic matter to degrade (Bartley 1996). Thus, local conditions within sediments must slow decay of kerogen and cells before the chert fully develops (Golubic 1976), or additional mechanisms may be needed to explain the rapid mineral precipitation required to preserve cellular shapes and delicate organic structures. One potential component missing from our understanding of this taphonomic window is the role that microbes themselves played in mineral precipitation and their own entombment in the earliest stages of organic preservation.

Recent work revealed that some marine cyanobacteria analogous to Proterozoic fossils can mediate the precipitation of amorphous, Mg-rich silica through a process of cation bridging when metabolic activity locally increases pH in microbial mats (Moore et al. 2020, 2021). In these microenvironments, cations help to bind negatively charged silicic acid to negatively charged organic surfaces (Moore et al. 2020, 2021). This cation-organic mediated mechanism of fossil preservation can occur even before silica concentrations reach saturation, meaning that they could precede more extensive chert development that required evaporation to highly concentrate silica. Studies of some modern environments and laboratory experiments have revealed similar associations among organic compounds and cations that may facilitate the formation of a range of authigenic minerals, from amorphous phases (Souza-Egipsy et al. 2005; Bontognali et al. 2010) to carbonates (Van Lith et al. 2003; Braissant et al. 2007; Bontognali et al. 2010, 2014; Krause et al. 2012; Kenward et al. 2013; Daye et al. 2019) and authigenic clays (Perri et al. 2018). It is possible that Proterozoic microbes interacted with their environments in a similar way to those observed in modern communities and experiments. Such interactions among cations, silica, and microbial surfaces may have been the key to early mineral nucleation and biosignature preservation in Proterozoic peritidal environments.

Here, we investigate Proterozoic chert deposits from four different fossiliferous formations (the Balbirini Dolomite and the Kotuikan, Debengda, and Duck Creek formations) to search for evidence of microbe-cation interactions preserved in Proterozoic peritidal cherts that can help to explain the excellent preservation of biosignatures (signs of past life) in these deposits. We measure and map the chemical composition of fossil kerogen and the surrounding rock matrix and reveal that kerogen is rarely preserved by micro- or cryptocrystalline quartz alone. Instead, kerogenous domains across all four formations are enriched in Ca and Mg and are embedded with nanoscopic, inorganic Ca-, Mg-, and Al-rich phases. By identifying these associations, we gain a more complete picture of the preservation of kerogen and fossils in Proterozoic peritidal

environments and identify a mechanism that may have enabled organic preservation in these environments. These results provide a deeper understanding of microbial-environmental interactions that characterized Proterozoic peritidal environments, including the roles of microbes in Mg, Ca, Al, and silica cycles and mineral formation.

GEOLOGIC SETTING

The four formations analyzed in this study represent a range of depositional environments, ages, and degrees of alteration, but all are predominantly peritidal carbonates with early diagenetic chert nodules, lenses, and laterally discontinuous beds. The Kotuikan Formation, northern Siberia (Fig. 1A), was deposited ca. 1500 Ma (Vorob'eva et al. 2015), and the Balbirini Dolomite, Australia (Fig. 1B), is constrained by zircon U-Pb ages of 1613 ± 4 and 1589 ± 3 Ma in its lower and upper parts, respectively (Page et al. 2000). Both contain superbly preserved microfossils (Oehler 1978; Sergeev et al. 1995). In both formations, the microbial lamination displays pustular textures and preserves predominantly *Eoentophysalis* fossils, coccoidal cyanobacteria that built intertidal microbial mats during the Proterozoic Eon (Fig. 1A, 1B), as they do today (Golubic and Hofmann 1976). Kerogen and fossils are densely packed in the microbial laminae. The laminae appear dark brown to opaque under transmitted light and are amber and reflective under incident light. The surrounding matrix is transparent, microcrystalline chalcedony and contains scattered clusters of fossils and abundant amorphous clots of dark brown to opaque kerogen (Fig. 1). Samples of both formations also contain layers of microcrystalline dolomite that alternate with the fossiliferous chert and contain microbial lamination, but no body fossils (Online Supplemental File Figure S1).

The Debengda Formation (ca. 1200–1300 Ma; Stanevich et al. 2009) was deposited in a more regularly inundated peritidal environment, preserving the sheaths of filamentous mat-builders (Sergeev et al. 1997). Cherts are microcrystalline and light brown to tan under transmitted light (Fig. 1C). They contain organic-rich microbial laminae and densely packed bundles of filamentous microfossils most commonly oriented parallel to the microbial laminae (Fig. 1c). In addition to these fossils, the cherts contain clots of dense, amorphous kerogen, similar to the kerogen seen in the Kotuikan and Balbirini samples (Fig. 1). Dispersed throughout the biosignature-preserving chert are fractures and primary pores filled by later diagenetic chert and dolomite. These regions truncate microbial lamination and are rimmed by rhombohedral dolomite and infilled by relatively coarsely crystalline chert (Fig. 1C). Isolated rhombohedral dolomite crystals are scattered throughout.

The Duck Creek Formation, which contains chert nodules deposited in shallow subtidal environments, is the oldest of the four formations analyzed (~ 1.9 Ga; Knoll and Barghoorn 1976; Grey and Thorne 1985; Knoll et al. 1988; Wilson et al. 2010; Schopf et al. 2015) and the most heavily altered. As a result, Duck Creek chert is blocky, with a coarser crystalline texture (dominated by 1–5 μm anhedral crystals) compared to the younger chert deposits. Under transmitted light, clots of kerogen in the Duck Creek Formation are distributed randomly throughout the chert matrix (Fig. 1D), but no fossils or microbial laminae were present in the samples analyzed in this study. The Duck Creek chert is frequently crosscut by veins of late diagenetic dolomite and contains abundant large rhombohedral dolomite crystals ($>15 \mu\text{m}$ across).

All four formations contain carbonate either as micritic layers that surround or alternate with the chert layers and nodules (e.g., Balbirini Dolomite and Kotuikan Formation; Online Supplemental File Figure S1), isolated 5–10 μm calcite and dolomite crystals scattered randomly throughout the chert matrix, or trails of larger rhombohedral dolomite crystals that cut through the chert. The isolated carbonate crystals scattered throughout the matrix may be early diagenetic precipitates or transported carbonate grains, but the coarse-crystalline dolomite trails crosscut the chert, likely reflecting late diagenetic alteration.

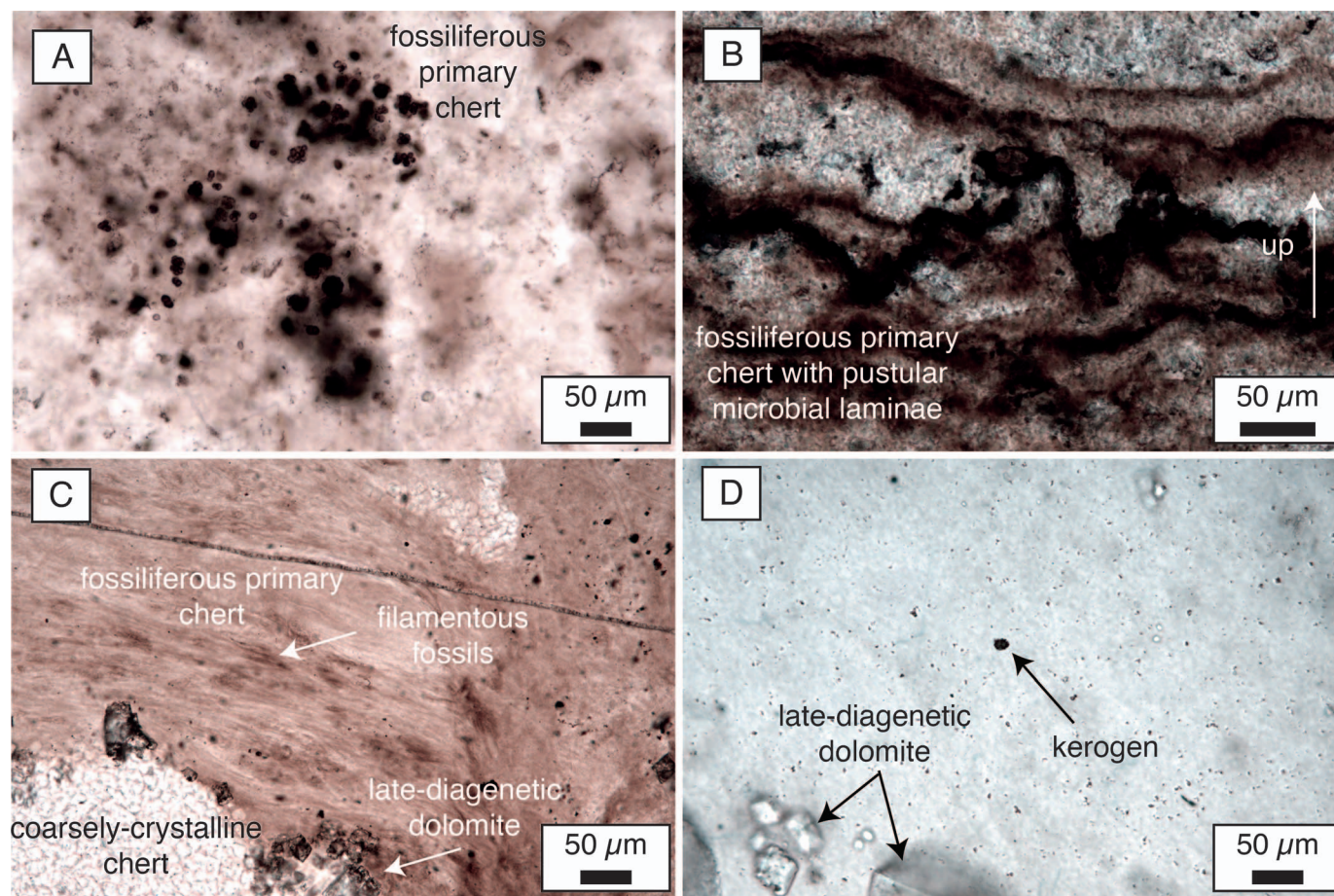


FIG. 1.—Transmitted light photomicrographs of thin sections. **A**) The Kotuikan Formation. **B**) The Balbirini Dolomite. **C**) The Debengda Formation. **D**) The Duck Creek Formation. Thin sections show examples of coccoidal microfossils with organic-rich walls (A, B), organic rich microbial lamination (B), filamentous microfossils (C), and kerogen clots (D) preserved in early diagenetic chert. All contain kerogen, and variable amounts of late diagenetic chert and both early and late diagenetic carbonate are found across the four formations.

METHODS

Preparation and Analysis of Chert Samples

Microfossiliferous and kerogen-preserving chert samples from four Proterozoic formations were selected and analyzed because they are known to contain early diagenetic chert from marine environments. All contain unambiguous biosignatures in the form of microbial laminae, microbial body fossils, and/or organic matter (Knoll and Barghoorn 1976; Oehler 1978; Grey and Thorne 1985; Knoll et al. 1988; Sergeev et al. 1995, 1997; Stanevich et al. 2009; Wilson et al. 2010; Schopf et al. 2015). Each sample was analyzed by scanning electron microscopy (SEM) with energy dispersive X-ray spectroscopy (EDS), Raman spectroscopy, and transmitted and reflected light microscopy. Each sample was prepared in two ways: (1) as freshly fractured surfaces mounted in indium or on SEM stubs, and (2) as polished thin sections. Freshly fractured surfaces provide a unique view of kerogen in three dimensions on the fractured areas, whereas polished thin sections show the kerogen and the associated grain boundaries of the surrounding minerals.

Fractured Surfaces

To prepare freshly fractured surfaces, small rock fragments were wrapped in cleaned foil that had been rinsed three times with 200 proof ethanol and fractured using an ethanol-cleaned chisel. Immediately

following fracturing, samples were rinsed with ethanol in a fume hood, wrapped loosely in ethanol-cleaned foil, and left to dry in a vacuum oven for one hour. Once dry, a fragment of each sample was mounted in a laminar flow hood with double-coated carbon conductive tape (Ted Pella Inc., Product #16084-7) onto 12.7 mm-diameter SEM stubs (Ted Pella Inc., Product #16111) and analyzed immediately to avoid contamination. These samples were analyzed on a Hitachi SU3500 variable pressure scanning electron microscope (VP-SEM) with an Oxford Instruments X-Max^N 150 mm² silicon drift energy dispersive spectroscopy (EDS) system at the NASA/Caltech Jet Propulsion Laboratory (JPL). Samples were analyzed without coating under variable pressure mode at 30 Pa. Regions of interest were imaged at 15 keV with 9–10 mm working distance at magnification of between 1.5k \times and 3k \times . These same regions were then analyzed by EDS using AZtec software (Oxford Instruments) at 15 keV. Each region of interest (ROI) was mapped at a resolution of 1024 \times 1024 pixels with 3 frames, 25 μ s dwell time, and between 1.5k \times and 3k \times magnification. Multiple phases within each ROI were also analyzed using single spot mode with the same instrument parameters.

In parallel, a second fragment of each cleaned, freshly fractured chert fragment was mounted in indium to avoid contamination from epoxy and was carbon coated and analyzed under vacuum on a ZEISS 1550VP Field Emission SEM (FESEM) with Oxford X-Max SDD X-ray (EDS) system at the California Institute of Technology Geology and Planetary Sciences Division Analytical Facility. Briefly, ethanol-cleaned indium was melted

into a cleaned aluminum disk and the cleaned rock fragments were mounted using a hydraulic press at JPL with ethanol cleaned foil covering the samples. The indium mount was carbon coated and analyzed at 15 keV under vacuum at 9–10 mm WD. ROIs were imaged at 2.5k \times to 3.5k \times magnification and 10 keV and analyzed with the same parameters by EDS using Aztec software. Elemental maps were generated at 512 \times 512 pixel to 1024 \times 1024 pixel resolution with 25 μ s dwell time. Spot analyses were performed using the same parameters.

Following SEM, uncoated fractured fragments on SEM stubs were analyzed by Raman spectroscopy using a Renishaw inViaTM confocal Raman microscope in the California Institute of Technology Geology and Planetary Sciences Division Mineral Spectroscopy Lab. Regions of interest were imaged and analyzed using a 20 \times objective lens with a 514 nm laser and 1800 line/mm grating. The analyses were performed with 1.7 mW laser power over a wavelength range from 50 cm^{-1} to 2500 cm^{-1} with 5–10 frames per spot. Data were analyzed using the Renishaw WiRE software to remove background and cosmic rays.

Polished Thin Sections

Standard polished 30 μ m thin sections were prepared by Wagner Petrographic. Thin sections were analyzed and imaged under transmitted and reflected light using a Leica DM6000B microscope in the abcLab at JPL. Polished sections were cleaned in the lab using a triple rinse of 200 proof ethanol and wrapped in ethanol-cleaned foil to dry for one hour in a vacuum drying oven. Once dry, samples were mounted in geological thin section holders (Ted Pella Inc., Product #15435-4) and samples were blown off with N₂ gas to ensure that no particulate matter remained on the sample surfaces before being analyzed by SEM. Like fractured surfaces, polished thin sections were analyzed and mapped under variable pressure mode at 30 Pa on the Hitachi SU3500 VP-SEM with Oxford Instruments X-Max^N 150 mm² silicon drift EDS system in the abcLab. Imaging and EDS analyses were carried out at 15 keV, magnification 1.5k \times to 2.5k \times , and mapping was performed at 1024 \times 1024 pixel resolution, 25 μ s dwell time, and 3 frames per region. Spot analyses were performed using the same parameters.

Precipitation Experiments

To test the role of cations in silica polymerization, precipitation experiments were carried out using artificial seawater medium (ASW; see Online Supplemental File Table S1 for medium recipe) with 90 ppm silica at pH 8.5–9. We tested two conditions in duplicate at pH 8.5–9: (1) 90 ppm silica ASW with 50 mM Mg²⁺, and (2) 90 ppm silica ASW with 10 mM Ca²⁺. Proterozoic [Mg²⁺] and [Ca²⁺] are difficult to constrain, and the ratio of Mg:Ca likely fluctuated throughout the Proterozoic (Riding 1982; Kaźmierczak et al. 2016). Therefore, we used modern seawater as a starting point and tested starting concentrations of 50 mM Mg²⁺ (condition 1) and 10 mM Ca²⁺ (condition 2). For each condition, we first titrated the artificial seawater to a pH of 8.5–9 using NaOH and then added additional Mg²⁺ or Ca²⁺ in the form of stock solutions of a 0.4 M Mg solution (made with MgSO₄) and a 1 M Ca solution (CaCl₂) until precipitation was observed. Control conditions contained no Mg²⁺ or Ca²⁺. We assessed the degree of silica polymerization aided by cations by measuring [SiO₂] before and after cation addition using the molybdate blue spectrophotometric assay after filtration through 0.05 μ m polycarbonate filters (Strickland and Parsons 1972). Precipitates were collected by filtration through 0.2 μ m polycarbonate filters that were then mounted on SEM stubs, and imaged and analyzed by SEM/EDS (see methods above) and deep-UV Raman Spectroscopy at the NASA/Caltech Jet Propulsion Laboratory. Deep-UV Raman measurements were done with 248.6 nm excitation using a custom-made spectrometer named MOBIUS (see Razzell Hollis et al. 2021 for a detailed description of the instrument).

Measurements were performed using an average laser energy of 1.7 μ J/pulse, 1200 pulses per acquisition, and 25 acquisitions were obtained to get a representative average spectrum. The purpose of these experiments was to observe whether silica could precipitate from seawater in the absence of Mg²⁺ or Ca²⁺, and to constrain the minimum concentrations of Mg²⁺ or Ca²⁺ that were necessary to initiate silica precipitation. Experiments were conducted in sterile 50 mL Falcon[®] Centrifuge Tubes at room temperature and pressure and were conducted under sterile conditions with no cells or organic compounds.

RESULTS

Characterization of Kerogen by Microscopy and Raman Spectroscopy

Reflected light photomicrographs and scanning electron micrographs of samples from all formations show that, although some contain well-preserved coccoidal and filamentous fossils and large clots of kerogen, only small patches of kerogen are exposed at the fracture or thin section surface. In backscattered electron (BSE) images, kerogen domains appear as fluffy, amorphous, dark regions that are generally less than 10 μ m across in any dimension (Fig. 2). These regions are distinct in color and texture from the angular microcrystalline chert matrix that surrounds them. EDS chemical maps and spot analyses of amorphous domains confirm that they are carbon-rich (Fig. 2) and distinct from the angular carbonate minerals that sometimes punctuate the chert and have higher intensity Ca and Mg peaks relative to the C peaks. On freshly fractured surfaces, the three-dimensional clots of kerogen are visible and highlight the contrast between the dark, amorphous, globular organic material and the angular, cleaved minerals that surround them (Fig. 2). BSE images of polished sections reveal smaller kerogenous domains—showing only a cross section through the domains similar to those observed in reflected light—and illustrate the grain boundaries of the micro- or cryptocrystalline quartz with the kerogen embedded within the matrix (Fig. 2).

Raman spectra from dark regions in all four chert samples display distinct peaks at \sim 1360 cm^{-1} and \sim 1600 cm^{-1} (Online Supplemental File Fig. S2), characteristic of the D (“disordered carbon”) and G (“graphitized carbon”) bands characteristic of kerogen. The two respective bands represent the more amorphous and more crystalline components of the kerogen’s macromolecular carbon and relate to its thermal maturity (Delarue et al. 2016). Spectra from spot analyses in the youngest formations (the Balbirini Dolomite and the Debengda and Kotuikan formations) reveal higher intensity G band peaks compared to the D band peaks, which are broad with shoulders at higher (the D6 band at \sim 1440 cm^{-1}) and lower (D5 band at \sim 1260 cm^{-1}) Raman shifts (Online Supplemental File Fig. S2). This suggests that the thermal maturity of the kerogen is consistent with peak temperatures of \sim 250°C (Henry et al. 2019). Kerogen in the Duck Creek Formation shows almost equivalent intensity D and G band peaks and both are narrow compared to the broad D band peaks of kerogen in samples from the younger formations (Online Supplemental File Figure S2). This suggests that the kerogen is more thermally mature than that of the younger formations (peak temperatures \sim 400°C; Henry et al. 2019), consistent with the age and alteration history of the Duck Creek Formation.

Fine Scale Analysis of Kerogen

To further characterize the elemental composition and preservation of the kerogen and surrounding matrix, we analyzed a minimum of 25 kerogenous domains from each formation with high-magnification imaging and elemental mapping. High-magnification BSE images and EDS spectra and maps revealed that none of the kerogenous domains from any of the four chert samples were preserved by micro- or cryptocrystalline quartz (SiO₂) alone. Instead, the organic matrices consistently contain elevated Ca and Mg content relative to the surrounding micro- or

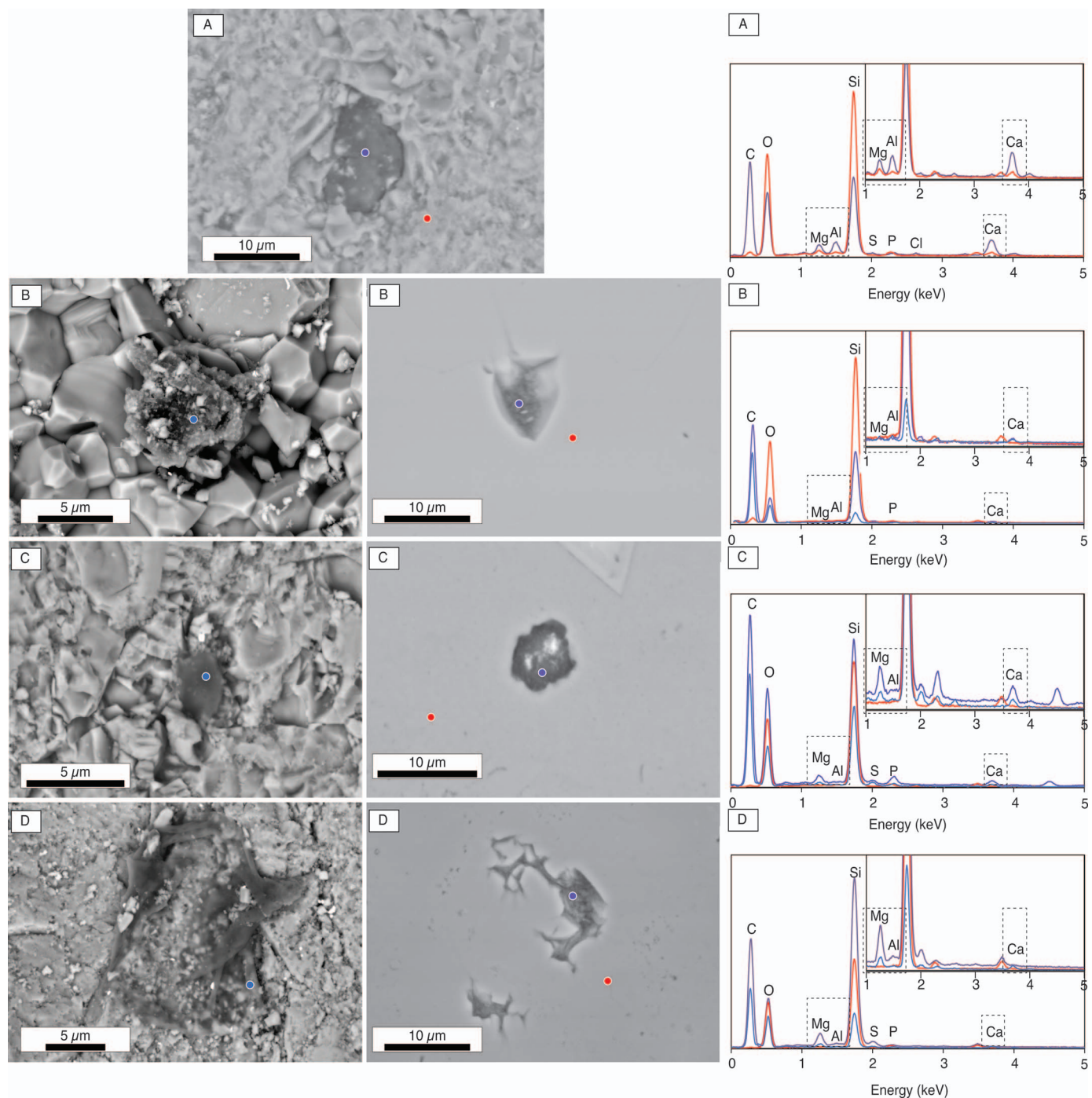


FIG. 2.—SEM BSE images showing organic domains preserved in early diagenetic chert. **A)** The Balbirini Dolomite. **B)** The Duck Creek Formation. **C)** The Debengda Formation. **D)** The Kotuikan Formation. Images show organic domains in thin section only for the Balbirini Dolomite because no hand samples were available for fracturing. For all other formations, an image from a freshly fractured surface shows an organic domain in three-dimensions with the chert crystals surrounding the kerogen and nanoscopic solid phases embedded in the kerogen (left). Polished thin sections show the organic domains embedded within the chert with sharp grain boundaries of the chert surrounding the organic matter and nanoscopic phases within the organic domains (middle). EDS spectra (right) reveal the presence of oxygen and silica as well as high intensity carbon peaks from the organic domains. Small magnesium, calcium, and aluminum peaks are present in the organic domains (blue from freshly fractured surfaces and purple from polished thin sections). The surrounding chert (red) does not contain the same high intensity carbon peaks and contains very little to no magnesium, calcium, and aluminum.

cryptocrystalline quartz and are embedded with inorganic, cation-rich nanoscopic phases (Fig. 3, Online Supplemental File Figs. S3–S5). The nanophases embedded within the kerogen are either angular crystals or colloidal or rounded particles tens to hundreds of nanometers in diameter

(Figs. 2, 3, Online Supplemental File Figs. S3–S5). The variability in composition in EDS chemical maps and $\sim 1 \mu\text{m}$ spot analyses show that these nanophases contain Mg, Ca, Al, or a combination of these elements along with Si and the organic C. The variability in the relative intensities of

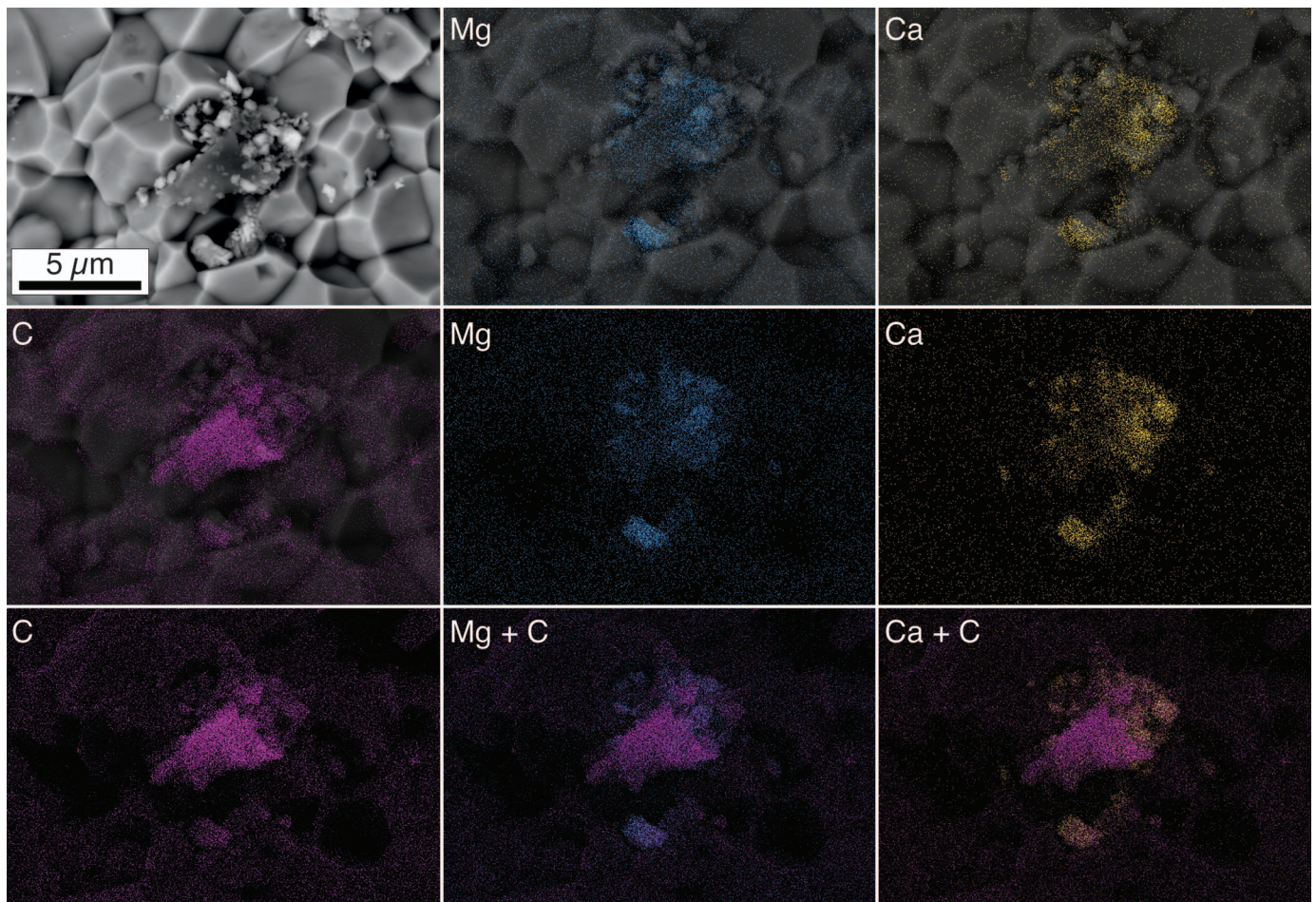


FIG. 3.—An example set of BSE images and EDS elemental maps of an organic domain preserved in the freshly fractured surface of the Duck Creek Formation. EDS map overlays show that the carbon (pink) is spatially correlated with the dark region of the BSE image. Overlays of magnesium (blue) and calcium (yellow) reveal cation enrichments in the organic material as faint magnesium and calcium maps that follow the organic carbon as well as bright spots of cation-rich nanophases embedded within the organic domain.

these elements in spots centered on different nanophases suggests that the phases represent a range of minerals and amorphous phases that may include carbonates (calcite and dolomite), clay minerals that contain a mix of Ca, Mg, and Al, and other nanoscopic, cation-rich silicate phases. We will refer to these collective inorganic, cation-rich, kerogen-bound, nanoscopic phases as “nanophases”.

In addition to the nanophases, the EDS analyses reveal that the kerogenous domains themselves are enriched in Ca and Mg. In EDS maps, organic-cation associations are seen as diffuse enrichments in Ca or Mg where the Ca and Mg maps are faint but spatially correlate with the brighter C maps (Fig. 3, Online Supplemental File Figs. S3–S5). Individual spot analyses of kerogenous material show that they contain Mg, Ca, or a combination of these elements. It is worth noting that these organic domains do not show enrichments in other major seawater cations such as Na or K. The spectra of kerogenous domains are distinct from the spot spectra of carbonate crystals that punctuate the chert because the former exhibit higher intensity of the C peaks relative to the Ca and Mg peaks (Fig. 2). Together, these results indicate that kerogen in these Proterozoic chert deposits is preserved in association with (1) organic-bound Ca and Mg and (2) nanophases containing Ca, Mg, and Al.

A statistical analysis of the cation composition of the nanophases and kerogen-bound Mg and Ca revealed trends in organic-cation associations across the formations. Of the 25 kerogenous domains analyzed in chert

from the Kotuikan Formation, 64% were Mg- and Ca-enriched, 24% were enriched in Mg only, and 12% were enriched in Ca only (Fig. 4). The nanophases embedded within kerogenous domains from the Kotuikan Formation were diverse, as well, with a high proportion of the 25 domains

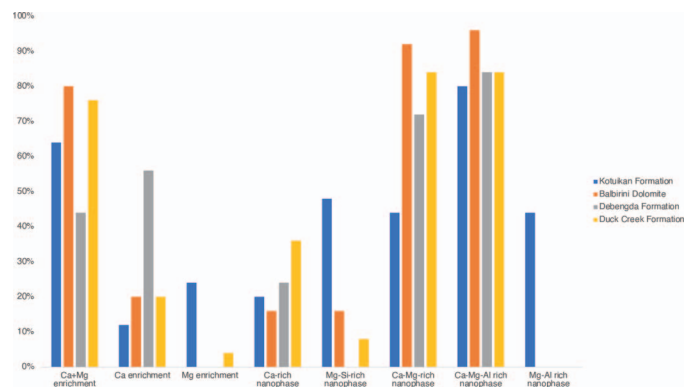


FIG. 4.—Histogram showing the percentages of the 25 organic domains from each formation that showed Ca enrichment, Mg enrichment, both Ca and Mg enrichment, and that contained Ca-rich nanophases, Mg-Si-rich nanophases, Ca-Mg-rich nanophases, Ca-Mg-Al-rich nanophases, and Mg-Al-rich nanophases.

containing Ca-Mg-Al-Si-rich phases (80% of the 25 domains analyzed), roughly equivalent proportions containing Mg-Si-rich (48% of the 25 domains analyzed), Ca-Mg-rich (44% of the 25 domains analyzed), and Mg-Al-Si-rich (44% of the 25 domains analyzed) phases, and some (20% of the 25 domains analyzed) containing Ca-rich phases (Fig. 4). Overall, both the kerogen and nanophases in the Kotuikan Formation showed evidence of Mg enrichment and elevated Ca. The Balbirini Dolomite showed similarly high proportions of kerogen-bound Ca and Mg, though a higher proportion of the 25 kerogenous domains analyzed showing both a Ca and Mg enrichment (80%) and Ca enrichment only (20%) and none showed only a Mg enrichment (Fig. 4). Domains from this formation contained dominantly Ca-Mg-rich phases (present in 92% of the 25 domains) and Ca-Mg-Al-Si-rich phases (present in 96% of the 25 domains) with some rare Ca-rich or Mg-Si-rich phases (both present in 16% of the 25 domains) (Fig. 4). Thus, the Balbirini Dolomite kerogen was characterized by enrichment in both Ca and Mg within the kerogen and mineral phases.

In contrast, kerogenous domains from the Debengda Formation are characterized predominantly by enrichment in Ca and Ca-rich phases. Of the 25 domains analyzed, 56% showed a Ca enrichment only, 44% showed both a Ca and Mg enrichment, and none showed only a Mg enrichment (Fig. 4). Domains were predominantly surrounded by Ca-Mg-Al-Si-rich phases (present in 84% of the 25 domains) and Ca-Mg-rich phases (present in 72% of the 25 domains) and some Ca-rich phases (present in 24% of the domains) (Fig. 4). The 25 kerogenous domains form the shallow subtidal Duck Creek Formation contained kerogenous domains characterized by both Ca and Mg enrichments (76% enriched in both Ca and Mg, 20% enriched in only Ca, and 4% enriched in only Mg) and had roughly equivalent proportion of domains that contained Ca-Mg-rich and Ca-Mg-Al-Si-rich phases (present in 84% of the 25 domains) with some Ca-rich phases (present in 36% of the 25 domains) and rare Mg-Si-rich phases (present in 8% of the 25 domains) (Fig. 4). These results indicated that kerogen from the Duck Creek Formation shows both Ca and Mg enrichment and abundant Mg-Ca-rich phases.

Precipitation Experiments

In seawater that is under or near silica saturation, even when silica concentrations are elevated through evaporation in peritidal environments, rapid precipitation may require cations and an initial nucleation step that precedes large-scale chert development (Krauskopf 1956; Iler 1979; Hinman and Lindstrom 1996; Rodgers et al. 2004; Orange et al. 2013). To explore the role of cations in silica precipitation, we conducted precipitation experiments using artificial seawater with 90 ppm silica buffered with NaHCO_3 and adjusted to pH 8.5–9 with 500 μL NaOH. Although this pH is elevated compared to modern seawater, we hypothesized that when silica was undersaturated, the precipitation of silicates aided by cations would require that the silicic acid ($\text{pK}^* = 9.38$; Hershey and Millero 1986) be deprotonated so that it could interact with other ions in solution (Tosca et al. 2011). This would be consistent with the well-documented ability of photosynthesis to locally increase the pH around a microbial mat (Ludwig et al. 2005) as well as pH increases associated with other anaerobic metabolisms (e.g., Tosca et al. 2011). Two conditions were tested, one with a starting concentration of 50 mM Mg^{2+} (C1) and one with a starting concentration of 10 mM Ca^{2+} (C2). Equilibrium speciation calculations using PHREEQC (Parkhurst and Appelo 2013) with thermodynamic data from the Minteq database (Allison et al. 1991), suggests that under these conditions, silica is present mostly as fully protonated silicic acid with some (6–7%) deprotonated silica acid and Mg and Ca are present primarily in the form of non-complexed divalent cations (Online Supplemental File Table S1).

Before adding Mg^{2+} and Ca^{2+} , no precipitation was observed in the seawater. When 50 mM Mg^{2+} was added (C1), some precipitation was

observed, and silica concentrations decreased by $15 \pm 1\%$. When an additional 10 mM Mg^{2+} was added (total $[\text{Mg}^{2+}] = 60$ mM), more small white precipitates formed in the seawater and silica concentrations decreased by $21 \pm 1\%$. SEM/EDS analyses revealed that the white, silica-rich precipitates were masses of nanoscopic, colloidal, Mg-rich silica particles (Fig. 5). Raman spectra of these precipitates showed a peak at 989.2 cm^{-1} characteristic of a silicate stretch mode (typically $985\text{--}1010 \text{ cm}^{-1}$) and two peaks at 1083 cm^{-1} and 1118.8 cm^{-1} , resembling multiple broad peaks that have been identified for cation-enriched silicate glasses which typically fall in the 1050 cm^{-1} to 1127 cm^{-1} range (Online Supplemental File Fig. S6). These peaks together are thus characteristic of cation-rich silicate (Mysen et al. 1982; Bellot-Gurlet et al. 2004), though likely nanocrystalline rather than truly amorphous based on the peak widths which are narrower than would be expected from an amorphous material. In the second condition, we did not observe precipitates until the addition of 20 mM Ca^{2+} (total $[\text{Ca}^{2+}] = 30$ mM), at which point white precipitates formed. Spectrophotometric assays showed an $8 \pm 2\%$ decrease in silica concentration after the addition of 20 mM Ca^{2+} while only a $5 \pm 3\%$ decrease in silica was measured when only 10 mM Ca was added. SEM/EDS revealed that the precipitates were mostly Ca-carbonates with rare Ca-silicates, and Raman spectra again showed peaks at 1008.5 cm^{-1} , representing a silicate stretch mode, and 1086.3 cm^{-1} and 1137.9 cm^{-1} , confirming the presence of nanocrystalline cation-enriched silicates; (Mysen et al. 1982; Bellot-Gurlet et al. 2004) alongside the carbonates (Online Supplemental File Fig. S7). PHREEQC modeling confirms that in C1, the solution is saturated with respect to Mg-silicates like sepiolite and talc alongside chalcedony (Online Supplemental File Table S1). Although the phase that we observed is not a crystalline Mg-silicate clay but is instead closer to a colloidal, nanocrystalline silicate, these results confirm the strong complexation between silica and Mg. In C2, models confirm that the solution is saturated with respect to aragonite and calcite alongside chalcedony (Online Supplemental File Table S1). Thus, for Ca^{2+} to aid in the polymerization of amorphous or nanocrystalline silicate, it must compete with calcium carbonate precipitation. By comparison, Mg^{2+} more readily complexes with silica to precipitate Mg-rich amorphous silicate.

DISCUSSION

Cation Enrichment in Primary Organic Matter Preserved in Early Diagenetic Chert

Cherts from all four formations host some combination of organic-rich microbial laminae, microbial body fossils, or discrete domains of kerogen distributed throughout the chert matrices. The abundance of kerogen visible in thin sections under transmitted and reflected light (Fig. 1), the identification of kerogenous domains embedded within the micro- or cryptocrystalline quartz using SEM/EDS in freshly fractured surfaces and thin sections (Fig. 2), and Raman spectra that identified kerogenous materials whose thermal maturity is consistent with the thermal history of their host rocks (Online Supplemental File Fig. S2; Knoll and Barghoorn 1976; Oehler 1978; Grey and Thorne 1985; Knoll et al. 1988; Sergeev et al. 1995, 1997; Stanevich et al. 2009; Wilson et al. 2010; Schopf et al. 2015; Henry et al. 2019) support the interpretation that the kerogen studied here is primary organic material representative of the microbes that inhabited these peritidal environments.

The presence of kerogen in chert from the Balbirini Dolomite and the Kotuikan, Debengda, and Duck Creek formations is consistent with the many previous studies that characterized the microfossils that they preserve (Knoll and Barghoorn 1976; Oehler 1978; Grey and Thorne 1985; Knoll et al. 1988; Sergeev et al. 1995, 1997; Stanevich et al. 2009; Wilson et al. 2010; Schopf et al. 2015). However, the ubiquitous presence of diffuse Ca, Mg, and a suite of inorganic, nanoscopic Ca-, Mg-, and Al-rich phases within the kerogen was previously undocumented. These cation enrich-

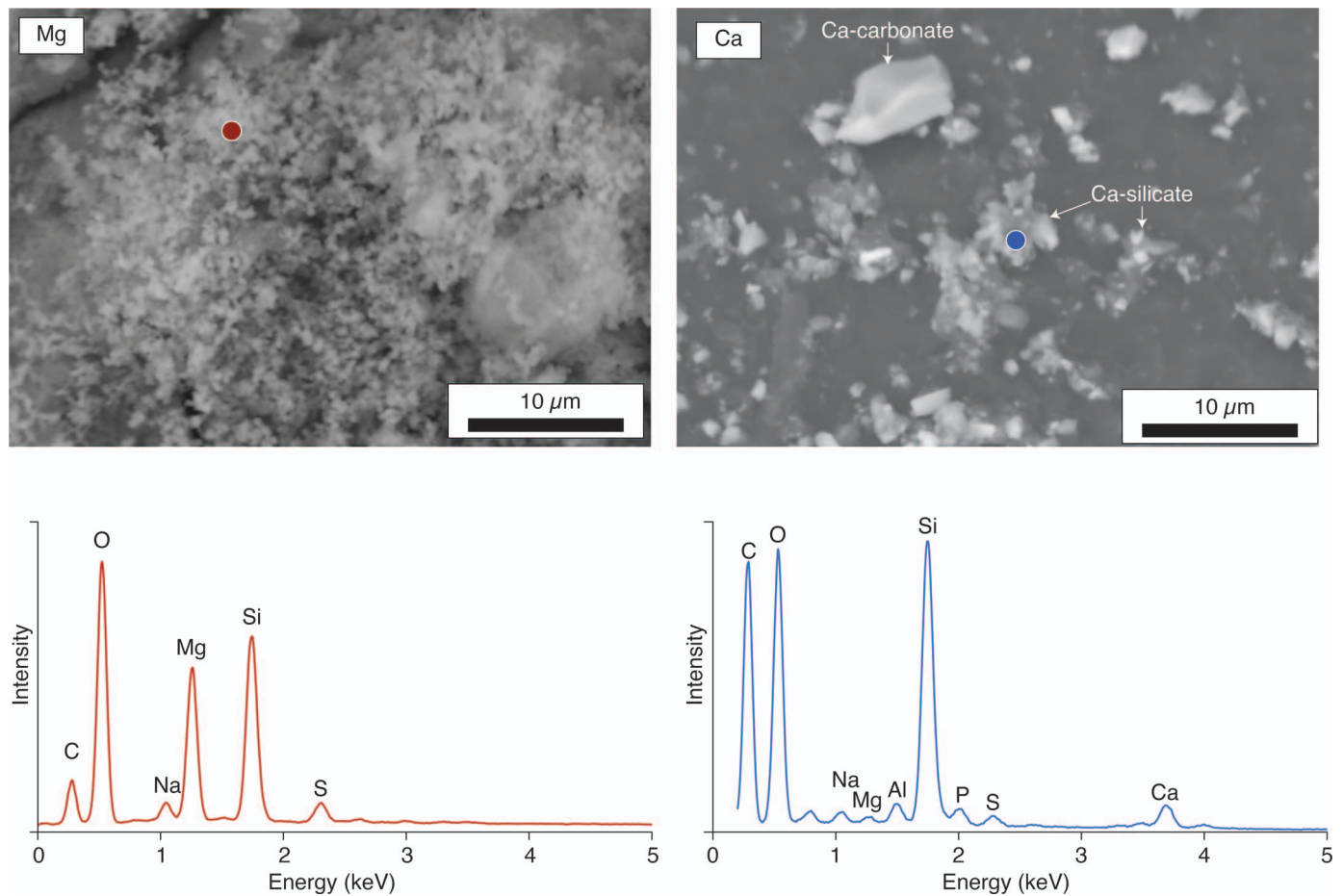


FIG. 5.—SEM BSE image of precipitates that formed under experimental conditions 1 (left) and 2 (right) after the addition of 60 mM Mg^{2+} and 30 mM Ca^{2+} , respectively, to seawater containing silica. Spectra from each show that the precipitates are primarily composed of Si and O with Mg (left, red) or Ca (right, blue). The precipitates are composed of nanoscopic colloidal Mg-rich silicate and Ca-rich silicate. In condition 2, Ca-carbonate crystals precipitated alongside the Ca-silicates.

ments and cation-rich phases suggest that kerogen in Proterozoic peritidal environments was not simply preserved by micro- or cryptocrystalline quartz but was instead originally stabilized by cation-rich silicate phases that pre-date extensive chert development. This is consistent with previously suggested chert precipitation mechanisms that rely on organic-cation interactions (Moore et al. 2021). Five hypotheses could explain the cation-organic associations: (1) Ca and Mg represent a primary component of the organic matrices (i.e., Ca- or Mg-rich organic compounds produced by some marine microbes in shallow environments); (2) Organic matter in Proterozoic marine environments effectively adsorbed and sequestered Mg^{2+} and Ca^{2+} from seawater and promoted nucleation of nanophases; (3) The nanophases are detrital clays and carbonates that were trapped and bound by the organic matrices; (4) Evaporation in peritidal environments locally concentrated silica and cations and promoted the precipitation of cation-rich minerals; and (5) Later diagenetic processes introduced cations into the chert after initial chert formation.

Hypotheses 1 and 2 are difficult to distinguish because both the biological production of cation-rich compounds (H1) and the sequestration of cations from seawater by organic compounds (H2) would result in cation-rich kerogen similar to what we observed by SEM/EDS (e.g., Fig. 3, Online Supplemental File Figs. S3–S5). Additionally, both explanations are plausible based on observations of modern marine organisms. Some modern marine microbes analogous to Proterozoic fossils are known to produce organic compounds containing cations (H1). For example, modern

marine *Spirulina* are helically coiled cyanobacteria analogous to fossil *Obruchevella*—a cyanobacterial fossil preserved in several Proterozoic chert deposits (Knoll and Ohta 1988; Butterfield and Rainbird 1998; Moore et al. 2017a; Shi et al. 2017). The modern organisms produce calcium spirulan, a calcium-containing sulfated polysaccharide (Lee et al. 1998). These and other cation-containing organic compounds may have similarly been produced by microbes that inhabited tidal environments during the Proterozoic.

Hypothesis 2 suggests that negatively charged surface groups in the extracellular polymeric substances (EPS) readily adsorbed specific cations from the seawater rather than being produced and exported by microbes as a primary organic component of their EPS. Previous studies have suggested that organic surfaces produced by a range of microbes have a net negative surface charge at circumneutral pH and can bind cations from solution (especially Mg and Ca; Douglas and Beveridge 1998; Dupraz et al. 2004; Souza-Egipsy et al. 2005; Krause et al. 2012; Kenward et al. 2013; Perri et al. 2018). Cation-binding capacity of organic surfaces is largely dependent on the protonation state of the dominant functional groups in microbial EPS as well as the pH of the solution and the concentrations of Mg^{2+} and Ca^{2+} . Some studies have even suggested that certain organic compounds and functional groups more readily bind cations than others (Kohn 1975; Bernkop-Schnürch and Krajčec 1998; Ouwerx et al. 1998; Lai et al. 2000; Dupraz et al. 2009; Bontognali et al. 2014; Moore et al. 2021) while other studies have suggested that certain organic compounds may preferentially bind either Mg^{2+} or Ca^{2+} . For

example, Moore et al. (2021) reported preferential Mg^{2+} binding by polysaccharide-rich EPS produced by modern analogs of *Eoentophysalis*, fossils preserved in the Balbirini Dolomite and Kotuikan Formation (Oehler 1978; Sergeev et al. 1995).

Whether primary components of the organic compounds (H1), adsorbed cations incorporated into the organic matrix (H2), or a combination of the two, the presence of Ca and Mg cations within the kerogen may explain the precipitation of nanophases around the organic matter, as well as the precipitation of chert. Although some of the nanophases may have been trapped and bound particles (H3), the sizes of these phases (< 500 nm) are much smaller than the detrital carbonate and clay grains present as inclusions in the chert (> 15 μm). Previous studies have similarly interpreted nanoscopic phases bound within microbial mats and organic matter as authigenic (Newman et al. 2016; Perri et al. 2018). In the case of purely abiotic processes (H4), evaporation would result in concentration of other major seawater cations within the organic matter and chert (Kolodny et al. 2005). Similarly, a late diagenetic process (H5) would likely result in cation enrichment throughout the chert. However, our results show local enrichments of only Ca and Mg with occasional Al in association with organic matter. The localized enrichment of Ca, Mg, and Ca-Mg-Al-rich phases specifically around kerogen and the absence of other species such as Na, K, or sulfate enrichment in the kerogen indicates that cation enrichments were not simply a byproduct of evaporation as chert precipitated abiotically around the organic matter. Rather, the binding of Ca and Mg may have predated evaporation and contributed to the initial nucleation of silicate phases. Additionally, the pristine preservation of microbial body fossils and the dense nature and low permeability of chert are inconsistent with extensive late diagenetic alteration of the chert. Thus, we favor either hypotheses 1, 2, or a combination of these to explain the Ca and Mg associations with the kerogen preserved across these chert formations. We suggest that these organic-cation associations may have promoted the precipitation of authigenic nanophases associated with the organic matter that preserved the biosignatures, as discussed below.

Cation Role in Nanophase Precipitation and Biosignature Preservation

Studies that investigated calcium carbonate and dolomite precipitation have shown that the adsorption of Mg^{2+} and Ca^{2+} by EPS may play a role in the nucleation of carbonate minerals (Riding 1991; Knoll et al. 1993; Douglas and Beveridge 1998; Van Lith et al. 2003; Dupraz et al. 2004; Braissant et al. 2007; Krause et al. 2012; Bontognali et al. 2014; Daye et al. 2019). It is possible that the specific binding affinity of certain microorganisms and organic compounds for Mg^{2+} ions may be the key to lowering the kinetic barrier to dolomite precipitation alongside metabolic processes like sulfate reduction (Van Lith et al. 2003; Roberts et al. 2013; Kenward et al. 2013; Bontognali et al. 2014). Similar cation-influenced mineral precipitation has also been extended to silicate and chert precipitation. Environmental studies have identified mixtures of carbonate, silicate, and amorphous phases in the EPS of biofilms from the sabkhas in Abu Dhabi and suggest that the biofilms adsorb ions like Ca^{2+} , Mg^{2+} , Al^{3+} , and dissolved silicic acid from solution (Perri et al. 2018). This is thought to result in the precipitation of nanoscopic authigenic carbonate, clays, and colloidal silicates ranging from tens to hundreds of nanometers in diameter (Perri et al. 2018). It has also been suggested that cations may play a specific role in the nucleation of silica both from supersaturated (Ferris et al. 1986, 1988; Schultze-Lam et al. 1993; Konhauser and Ferris 1996; Konhauser et al. 2001) and undersaturated (Urrutia and Beveridge 1993, 1994; Souza-Egipsy et al. 2005; Moore et al. 2020, 2021) solutions by acting as cation bridges that facilitates the binding of negatively charged silicic acid by negatively charged organic surfaces. Abiotic studies have additionally proposed that cations may play a fundamental role in the polymerization of silica from undersaturated

solutions even in the absence of organic compounds (Owen 1975; Iler 1979).

Although the precipitation of micro- to cryptocrystalline quartz and other pure SiO_2 phases is most favorable when concentrations are above saturation and $pH < 8-8.5$, the formation of cation-rich silica phases from silica-undersaturated solutions requires a different set of conditions. In seawater that is undersaturated with respect to silica, silica alone will not precipitate spontaneously. Indeed, even near amorphous silica saturation, silica precipitation is minimal and the precipitates are poorly cemented and often not stable over the course of days as pH and temperature fluctuations dissolve and reprecipitate the thin, friable films (Shimada and Tarutani 1980; Hinman and Lindstrom 1996; Orange et al. 2013; Wilmeth et al. 2021). However, if the pH is elevated such that some of the silicic acid is deprotonated and carries a negative charge, Mg and Ca—present as divalent cations—can aid in polymerization by interacting with silicic acid (Owen 1975; Iler 1979; Rodgers et al. 2004). Our precipitation experiments confirm that uncomplexed cations—specifically Mg^{2+} and Ca^{2+} —can facilitate the nucleation of cation-rich silica from seawater at room temperature and pressure when silica concentrations are below amorphous saturation. As these cations become more concentrated, progressively more silica precipitation is observed in the form of nanoscopic silica phases. Past studies have demonstrated that cations like Na^+ (Dove et al. 2019) and Ca^{2+} and Mg^{2+} (Dove and Craven 2005) influence silica polymerization by increasing the nucleation rate of silica polymers and creating a negative surface charge of the resulting colloidal silica. Although our experiments showed only the initial phase of poorly crystalline, cation-rich silica polymerization, a similar initial stage of polymerization may have played a role in biosignature preservation and chert development in Proterozoic environments. The rapid initial polymerization of silica driven by cations could occur on timescales conducive to the preservation of the organic matter before degradation. These initial negatively charged phases could then act as nucleation points to template further silica polymerization and eventual crystallization as the silica concentrations progressively increased through evaporitic processes.

The need for $pH > 7$ is consistent with previous studies that assessed the role of photosynthetic activity in precipitation (Moore et al. 2020, 2021). Photosynthesis as well as other metabolic activity like anaerobic respiration could have all driven pore water pH to values > 7 (Tosca et al. 2011). These pH values and the requirement for Mg^{2+} and Ca^{2+} at elevated concentrations suggest an additional role for microbes and organic matter in this process of rapid, initial mineral nucleation and organic preservation. If Proterozoic marine concentrations of Mg^{2+} and Ca^{2+} were near or below modern seawater, some mechanism may have been necessary to concentrate these cations locally and facilitate the rapid local polymerization of amorphous silicate around cells. Based on these results and the previously demonstrated ability of organic surfaces to sequester and concentrate cations from seawater, it is possible that microbes in Proterozoic tidal environments promoted cation-rich silica precipitation both by elevating local pH beyond 7 and by sequestering cations to locally concentrate Mg^{2+} and Ca^{2+} enough to polymerize cation-rich silica. These combined microbial influences on the local chemical environment can explain the rapid polymerization of amorphous, cation-rich silica around organic matter. Once nucleated, this organic-bound, cation-rich silica may have been key to preserving biosignatures before organic matter was degraded in living, metabolizing microbial mat communities. This could have been especially important for the preservation of cell sheaths and envelopes represented by the body fossils that we see today.

Chert Preservation Aided by Cations

Since the discovery of microfossils in chert from the Paleoproterozoic Gunflint Formation (Tyler and Barghoorn 1954), chert has been recognized as an exceptional source of information on early life. Its hardness, low

permeability, and resistance to recrystallization all contribute to chert's capacity to preserve organic matter, including microfossils, over long time spans. Equally, it has long been hypothesized that while chert enables preservation in the long run, other processes must have aided preservation during early diagenesis (e.g., Knoll 1985). Based on evidence that suggests a need for > 300 ppm silica concentrations to precipitate extensive stable, dense chert development which may take time (Krauskopf 1956; Chan 1989; Hinman and Lindstrom 1996; Orange et al. 2013; Wilmeth et al. 2021), evaporation alone may not have been enough to preserve organic matter before degradation. Some have suggested that organic material may act as a template that bonds to silicic acid, initiates silica polymerization, and leads to its localized nucleation and preservation of organic matter (Leo and Barghoorn 1976; Knoll 1985; Renaut et al. 1998). We expand this mechanism and propose that the nucleation of silica and preservation of organic matter involves not only interactions among organic surfaces and silica but also cations and cation-rich phases. All of our samples contain kerogen preserved by cation-rich phases that predate the chert and likely preserved the kerogen before large-scale formation of amorphous silica and crystallization of chert. Indeed, these initial cation-rich phases may have laid the foundation for localized chert precipitation. Once the initial, amorphous, cation-rich silica nucleated on the organic matter in a manner similar to the formation of nanocrystalline, cation-rich, colloidal silica observed in our precipitation experiments, further polymerization of silica onto those initial nucleation points could proceed as evaporitic or other processes in these environments increased the concentration of silica to form large-scale amorphous silica deposits. In this way, the organic compounds provided a template for amorphous silica to precipitate through cation interactions. The amorphous precipitates would then dehydrate and crystallize over time to form the chert that we see today.

Perri et al. (2018) noted that the initial nanoscopic carbonate phases in microbial mats that colonize hypersaline sabkhas are not pure Mg/Ca carbonate, but instead always contain some Si and Al. One important difference between these environments and Proterozoic tidal environments is that the concentration of [SiO₂] in the Proterozoic seawater was likely much higher than that of the modern sabkhas. Although nanoscopic phases enriched in Ca and Mg may rapidly form in microbial mats and represent the first key nucleation step to preserving the organic matter, it is possible that the constant accumulation and incorporation of silica into these initial phases may ultimately result in the dominance of chert formation if the concentration of dissolved SiO₂ was high enough. Abiotic processes like evaporation likely concentrated the dissolved silica locally in these peritidal environments, driving chert formation and maturation after the nucleation of cation-rich silica phases and the preservation of the biosignatures. This would explain the prevalence of chert-hosted biosignatures in peritidal carbonates rather than carbonates that formed in deeper marine environments.

Cation Variability across Formations

The dominant cations associated with kerogen in each formation matched the compositions of the nanoscopic mineral phases embedded in the same organic domains, but there were differences in Mg and Ca enrichment between formations and depositional environments. Three formations revealed both Ca and Mg enrichment while the Debengda Formation showed higher Ca enrichment relative to Mg. The variability in Ca and Mg in the organic matter and nanophases may reflect slight differences in the organic surfaces, their cation contents or binding capacities, the chemistry of the environments where each formed, or a combination of these biological and abiotic factors at the time of preservation. Our precipitation experiments reveal that the concentrations of Mg²⁺ and Ca²⁺ ions in the seawater exert a strong control on the initial phases that nucleate around organic matter. The prevalence of both Mg and Ca in organic matter and nanophases preserved in the Balbirini, Kotuikan,

and Duck Creek cherts suggest that when both Mg and Ca are present, both may be incorporated into amorphous silica as it precipitates. Although the addition of Mg²⁺ to silica-rich seawater resulted in rapid precipitation of Mg-rich silica, Ca²⁺ concentrations had to be concentrated three times higher than that of modern seawater to form amorphous, cation-rich silica alongside Ca-carbonate. Thus, the dominance of Ca in the Debengda Formation suggests the local pore water had a higher Ca²⁺:Mg²⁺ ratio or total Ca²⁺ concentrations relative to the other environments, allowing for the precipitation of Ca-rich silicate alongside carbonate. Alternatively, the microbes that inhabited the peritidal realm in which the Debengda Formation was deposited may have produced Ca-rich EPS (Lee et al. 1998) or other organic compounds that preferentially adsorbed Ca from seawater. Either of these controls, or a combination of the biological and abiotic factors, could explain the Ca enrichment in the organic matter from the Debengda Formation.

Post-Depositional Alteration of Authigenic Silicates

The lack of Al associated with the organic matrices in the four chert formations analyzed in this study suggests that this cation, unlike Ca and Mg, was not initially adsorbed to organic material. Instead, the consistent presence of Al-rich phases across all formations while Ca and Mg enrichments varied suggests that the incorporation of Al may represent a later stage of diagenesis common to all four environments, but still prior to bulk chert formation. Studies of modern sediments in the Amazon River Delta and diagenesis of biogenic silica have found that as opaline silica dissolves, authigenic clays form through the incorporation of aluminum into the silica sourced from terrigenous material carried into the ocean (Dixit et al. 2001; Michalopoulos and Aller 2004). If the incorporation of Mg and Ca into organic matrices in the Balbirini, Kotuikan, Debengda, and Duck Creek sediments led to the precipitation of carbonates as well as Ca- and Mg-rich amorphous silica nanophases, it is possible that secondary transformation of the amorphous silica phases resulted in the formation of authigenic clays that contain Ca, Mg, Al, and Si. This would explain the localization of Al-clays associated with cation-rich silicates in kerogen. However, this explanation requires a source of Al³⁺. The analyzed chert deposits generally do not contain abundant detrital siliciclastic material other than the phases associated with the kerogen, indicating that these were not siliciclastic-rich depositional environments. It is possible that local weathering of clays or other detrital Al-rich minerals near these environments may have resulted in local release of Al³⁺ into the peritidal environments. This Al³⁺ could rapidly react with the silicates to form alteration products such as cation-rich silicate clays around organic surfaces before the extensive precipitation of chert. Studies have demonstrated the exceptional ability of clays to preserve microbial organisms in carbonate environments (Moore et al. 2017b) in siliciclastic environments, some of which are calcium enriched relative to the bulk clay composition (Kennedy et al. 2002, 2014; Newman et al. 2016, 2017; Anderson et al. 2020). It is also possible that the localization of Al-silicates around kerogen reflects preferential binding of rare fluxes of Al-minerals (e.g., through airborne dust) onto organic surfaces. Whether detrital or authigenic, the presence of Al-rich phases around the kerogen is consistent with the preservation of kerogen by clays, especially those that showed enrichment in calcium (Newman et al. 2016).

CONCLUSIONS

This study reveals a previously unexplored relationship among cations, silica, and kerogen preserved in Proterozoic chert that helps explain the exquisite preservation of biosignatures in these deposits. Our results and previous studies have highlighted the ability of organic compounds to bind and accumulate cations from solution, the ability of this sequestration process to promote mineral and nanophase nucleation in and around

organic surfaces, and the role of cations in the polymerization of silica. This study adds an important dimension to our understanding of biosignature preservation. We find evidence for the roles of these combined biological and abiotic processes in the preservation of organic matter and microfossils in Proterozoic peritidal environments.

Organic matter preservation in Proterozoic peritidal environments may have been more complex than the simple formation of chert around microbial mats. Our chemical analyses of the organic biosignatures and the associated inorganic nanophases that preserve them show that these biosignatures are initially preserved by cation-rich phases that subsequently became encapsulated in chert. Based on the enrichments in Mg and Ca in the kerogen and the presence of cation-rich carbonate and silicate phases embedded within the kerogen, we suggest that cations were either a component of the organic matter or were sequestered by the organic matter in these environments. The sequestration of cations by organic surfaces and metabolic activity that increased local pH may have locally concentrated cations and created microenvironments that favored rapid nucleation and precipitation of nanophases. This process and the interactions among organic matter, cations in solution, and silica may have laid the foundation for organic preservation, stabilizing the organic material rapidly before it could be degraded and enabling exceptional preservation of organic matter and microbial fossils in these environments. The organomineral associations formed during the initial stages likely acted as templates for more extensive chert development in evaporitic peritidal environments, but the microbes had to first lay the foundation for their own entombment and preservation.

ACKNOWLEDGMENTS

We thank the National Aeronautics and Space Administration and the Jet Propulsion Laboratory, California Institute of Technology, for funding. The research was carried out, in part, at the Jet Propulsion Laboratory, California Institute of Technology, under a contract with the National Aeronautics and Space Administration (80NM0018D0004). We also thank the Simons Foundation for funding through the Simons Collaboration on the Origins of Life to JPG and TB. Additional thanks to D. Hutkin for support. We also thank two anonymous reviewers for helpful questions, comments, and suggestions.

SUPPLEMENTAL MATERIAL

Data are available from the PALAIOS Data Archive:
<https://www.sepm.org/supplemental-materials>.

REFERENCES

- ALLISON, J.D., BROWN, D.S., AND NOVO-GRADAC, K.J., 1991, MINTEQA2/PRODEFA2, A geochemical assessment model for environmental systems: Version 3.0 user's manual: Environmental Research Laboratory, Office of Research and Development, U.S. Environmental Protection Agency User Manual, 100 p.
- ANDERSON, R.P., TOSCA, N.J., CINQUE, G., FROGLEY, M.D., LEKKAS, I., AKEY, A., HUGHES, G.M., BERGMANN, K.D., KNOLL, A.H., AND BRIGGS, D.E.G., 2020, Aluminosilicate haloes preserve complex life approximately 800 million years ago: *Interface Focus*, v. 10, article 20200011, doi: 10.1098/rsfs.2020.0011.
- BARTLEY, J.K., 1996, Actualistic taphonomy of cyanobacteria: implications for the Precambrian fossil record: *PALAIOS*, v. 11, p. 571–586, doi: 10.2307/3515192.
- BELLOTT-GURLET, L., BOURDONNÉ, F.-X.L., POUPÉAU, G., AND DUBERNET, S., 2004, Raman micro-spectroscopy of western Mediterranean obsidian glass: one step towards provenance studies?: *Journal of Raman Spectroscopy*, v. 35, p. 671–677, doi: 10.1002/jrs.1195.
- BERNKOP-SCHNÜRCH, A. AND KRAJICEK, M.E., 1998, Mucoadhesive polymers as platforms for peroral peptide delivery and absorption: synthesis and evaluation of different chitosan–EDTA conjugates: *Journal of Controlled Release*, v. 50, p. 215–223, doi: 10.1016/S0168-3659(97)00136-3.
- BONTOGNALLI, T.R.R., MCKENZIE, J.A., WARTHMAN, R.J., AND VASCONCELOS, C., 2014, Microbially influenced formation of Mg-calcite and Ca-dolomite in the presence of exopolymeric substances produced by sulphate-reducing bacteria: *Terra Nova*, v. 26, p. 72–77, doi: 10.1111/ter.12072.
- BONTOGNALLI, T.R.R., VASCONCELOS, C., WARTHMAN, R.J., BERNASCONI, S.M., DUPRAZ, C., STROHMENGER, C.J., AND MCKENZIE, J.A., 2010, Dolomite formation within microbial mats in the coastal sabkha of Abu Dhabi (United Arab Emirates): *Sedimentology*, v. 57, p. 824–844, doi: 10.1111/j.1365-3091.2009.01121.x.
- BRAISSANT, O., DECHO, A.W., DUPRAZ, C., GLUNK, C., PRZEKOP, K.M., AND VISSCHER, P.T., 2007, Exopolymeric substances of sulfate-reducing bacteria: interactions with calcium at alkaline pH and implication for formation of carbonate minerals: *Geobiology*, v. 5, p. 401–411, doi: 10.1111/j.1472-4669.2007.00117.x.
- BUTTERFIELD, N.J., 2015, Proterozoic photosynthesis—a critical review: *Palaeontology*, v. 58, p. 953–972, doi: 10.1111/pala.12211.
- BUTTERFIELD, N.J. AND RAINBIRD, R.H., 1998, Diverse organic-walled fossils, including “possible dinoflagellates,” from the early Neoproterozoic of arctic Canada: *Geology*, v. 26, p. 963–966.
- CHAN, S.H., 1989, A review on solubility and polymerization of silica: *Geothermics*, v. 18, p. 49–56, doi: 10.1016/0375-6505(89)90009-6.
- CONLEY, D.J., FRINGS, P.J., FONTORBE, G., CLYMANS, W., STADMARK, J., HENDRY, K.R., MARRON, A.O., AND DE LA ROCHA, C.L., 2017, Biosilicification drives a decline of dissolved Si in the oceans through geologic time: *Frontiers in Marine Science*, v. 4, p. 397, doi: 10.3389/fmars.2017.00397.
- DAYE, M., HIGGINS, J., AND BOSAK, T., 2019, Formation of ordered dolomite in anaerobic photosynthetic biofilms: *Geology*, v. 47, p. 509–512, doi: 10.1130/G45821.1.
- DELARUE, F., ROUZAUD, J.-N., DERENNE, S., BOURBIN, M., WESTALL, F., KREMER, B., SUGITANI, K., DELDICQUE, D., AND ROBERT, F., 2016, The Raman-derived carbonization continuum: a tool to select the best preserved molecular structures in Archean kerogens: *Astrobiology*, v. 16, p. 407–417, doi: 10.1089/ast.2015.1392.
- DEMOULIN, C.F., LARA, Y.J., CORNET, L., FRANÇOIS, C., BAURAIN, D., WILMOTTE, A., AND JAVAU, E.J., 2019, Cyanobacteria evolution: insight from the fossil record: *Free Radical Biology and Medicine*, v. 140, p. 206–223, doi: 10.1016/j.freeradbiomed.2019.05.007.
- DIXIT, S., VAN CAPPELLEN, P., AND VAN BENNEKOM, A.J., 2001, Processes controlling solubility of biogenic silica and pore water build-up of silicic acid in marine sediments: *Marine Chemistry*, v. 73, p. 333–352, doi: 10.1016/S0304-4203(00)00118-3.
- DOUGLAS, S. AND BEVERIDGE, T.J., 1998, Mineral formation by bacteria in natural microbial communities: *FEMS Microbiology Ecology*, v. 26, p. 79–88, doi: 10.1111/j.1574-6941.1998.tb00494.x.
- DOVE, P.M. AND CRAVEN, C.M., 2005, Surface charge density on silica in alkali and alkaline earth chloride electrolyte solutions: *Geochimica et Cosmochimica Acta*, v. 69, p. 4963–4970, doi: 10.1016/j.gca.2005.05.006.
- DOVE, P.M., HAN, N., AND WALLACE, A.F., 2019, Systematic dependence of kinetic and thermodynamic barriers to homogeneous silica nucleation on NaCl and amino acids: *Journal of Materials Research*, v. 34, p. 442–455, doi: 10.1557/jmr.2018.474.
- DUPRAZ, C., REID, R.P., BRAISSANT, O., DECHO, A.W., NORMAN, R.S., AND VISSCHER, P.T., 2009, Processes of carbonate precipitation in modern microbial mats: *Earth-Science Reviews*, v. 96, p. 141–162.
- DUPRAZ, C., VISSCHER, P.T., BAUMGARTNER, L.K., AND REID, R.P., 2004, Microbe-mineral interactions: early carbonate precipitation in a hypersaline lake (Eleuthera Island, Bahamas): *Sedimentology*, v. 51, p. 745–765, doi: 10.1111/j.1365-3091.2004.00649.x.
- FERRIS, F.G., BEVERIDGE, T.J., AND FYFE, W.S., 1986, Iron-silica crystallite nucleation by bacteria in a geothermal sediment: *Nature*, v. 320, p. 609–611, doi: 10.1038/320609a0.
- FERRIS, F.G., FYFE, W.S., AND BEVERIDGE, T.J., 1988, Metallic ion binding by *Bacillus subtilis*: implications for the fossilization of microorganisms: *Geology*, v. 16, p. 149–152, doi: 10.1130/0091-7613(1988)016<0149:MIBBBS>2.3.CO;2.
- GOLUBIC, S., 1976, Chapter 4.2, Taxonomy of Extant Stromatolite-Building Cyanophytes, in Walter, M.R. (ed.), *Developments in Sedimentology: Stromatolites*, Elsevier, p. 127–140. <https://www.sciencedirect.com/science/article/pii/S0070457108711336>. Checked January 2022.
- GOLUBIC, S. AND HOFMANN, H.J., 1976, Comparison of Holocene and Mid-Precambrian Entophysalidaceae (Cyanophyta) in stromatolitic algal mats: cell division and degradation: *Journal of Paleontology*, v. 50, p. 1074–1082.
- GREY, K. AND THORNE, A.M., 1985, Biostratigraphic significance of stromatolites in upward shallowing sequences of the early proterozoic duck creek dolomite, Western Australia: *Precambrian Research*, v. 29, p. 183–206, doi: 10.1016/0301-9268(85)90068-3.
- HENRY, D.G., JARVIS, I., GILLMORE, G., AND STEPHENSON, M., 2019, Raman spectroscopy as a tool to determine the thermal maturity of organic matter: application to sedimentary, metamorphic and structural geology: *Earth-Science Reviews*, v. 198, article 102936, doi: 10.1016/j.earscirev.2019.102936.
- HERSHEY, J.P. AND MILLERO, F.J., 1986, The dependence of the acidity constants of silicic acid on NaCl concentration using Pitzer's equations: *Marine Chemistry*, v. 18, p. 101–105, doi: 10.1016/0304-4203(86)90079-4.
- HINMAN, N.W. AND LINDSTROM, R.F., 1996, Seasonal changes in silica deposition in hot springs systems: *Chemical Geology*, v. 132, p. 237–246, doi: 10.1016/S0009-2541(96)00060-5.
- ILER, K.R., 1979, *The Chemistry of Silica: Solubility, Polymerization, Colloid and Surface Properties and Biochemistry of Silica*: John Wiley and Sons, Chichester, 896 p.
- JONES, B., KONHAUSER, K.O., RENAUT, R.W., AND WHEELER, R.S., 2004, Microbial silicification in Iodine Pool, Waimangu geothermal area, North Island, New Zealand: implications for recognition and identification of ancient silicified microbes: *Journal of the Geological Society*, v. 161, p. 983–993, doi: 10.1144/0016-764903-172.

- KAZMIERCZAK, J., ITTEKKOT, V., AND DEGENS, E.T., 2016, Biocalcification through time: environmental challenge and cellular response: *PalZ*, v. 59, p. 15, doi: 10.1007/BF02985996.
- KENNEDY, M.J., LÖHR, S.C., FRASER, S.A., AND BARUCH, E.T., 2014, Direct evidence for organic carbon preservation as clay-organic nanocomposites in a Devonian black shale; from deposition to diagenesis: *Earth and Planetary Science Letters*, v. 388, p. 59–70, doi: 10.1016/j.epsl.2013.11.044.
- KENNEDY, M.J., PEVEAR, D.R., AND HILL, R.J., 2002, Mineral surface control of organic carbon in black shale: *Science*, v. 295, p. 657–660, doi: 10.1126/science.1066611.
- KENWARD, P.A., FOWLE, D.A., GOLDSTEIN, R.H., UESHIMA, M., GONZÁLEZ, L.A., AND ROBERTS, J.A., 2013, Ordered low-temperature dolomite mediated by carboxyl-group density of microbial cell walls: *AAPG Bulletin*, v. 97, p. 2113–2125, doi: 10.1306/05171312168.
- KNOLL, A.H., 2008, Cyanobacteria and Earth History, in A. Herrero and E. Flores (eds.), *The Cyanobacteria: Molecular Biology, Genomics and Evolution*: Caister Academic Press, Poole, UK, 514 p.
- KNOLL, A.H., 1985, Exceptional preservation of photosynthetic organisms in silicified carbonates and silicified peats: *Philosophical Transactions of the Royal Society of London B, Biological Sciences*, v. 311, p. 111–122, doi: 10.1098/rstb.1985.0143.
- KNOLL, A.H. AND BARGHOORN, E.S., 1976, A gunflint-type microbiota from the Duck Creek dolomite, Western Australia: *Origins of Life*, v. 7, p. 417–423, doi: 10.1007/BF00927937.
- KNOLL, A.H., FAIRCHILD, L.J., AND SWETT, K., 1993, Calcified microbes in neoproterozoic carbonates: implications for our understanding of the Proterozoic/Cambrian transition: *PALAIOS*, v. 8, p. 512–525, doi: 10.2307/3515029.
- KNOLL, A.H. AND GOLUBIC, S., 1979, Anatomy and taphonomy of a Precambrian algal stromatolite: *Precambrian Research*, v. 10, p. 115–151, doi: 10.1016/0301-9268(79)90022-6.
- KNOLL, A.H. AND OHTA, Y., 1988, Microfossils in metasediments from Prins Karls Forland, western Svalbard: *Polar Research*, v. 6, p. 59–67, doi: 10.3402/polar.v6i1.6846.
- KNOLL, A.H., STROTHER, P.K., AND ROSSI, S., 1988, Distribution and diagenesis of microfossils from the lower Proterozoic Duck Creek Dolomite, Western Australia: *Precambrian Research*, v. 38, p. 257–279, doi: 10.1016/0301-9268(88)90005-8.
- KOHN, R., 1975, Ion binding on polyuronates—alginate and pectin: *Pure and Applied Chemistry*, v. 42, p. 371–397, doi: 10.1351/pac197542030371.
- KOLODNY, Y., CHAUSSIDON, M., AND KATZ, A., 2005, Geochemistry of a chert breccia: *Geochimica et Cosmochimica Acta*, v. 69, p. 427–439, doi: 10.1016/j.gca.2004.07.010.
- KONHAUSER, K.O. AND FERRIS, F.G., 1996, Diversity of iron and silica precipitation by microbial mats in hydrothermal waters, Iceland: implications for Precambrian iron formations: *Geology*, v. 24, p. 323, doi: 10.1130/0091-7613(1996)024<0323:DOIASP>2.3.CO;2.
- KONHAUSER, K.O., PHOENIX, V.R., BOTTRELL, S.H., ADAMS, D.G., AND HEAD, I.M., 2001, Microbial-silica interactions in Icelandic hot spring sinter: possible analogues for some Precambrian siliceous stromatolites: *Sedimentology*, v. 48, p. 415–433, doi: 10.1046/j.1365-3091.2001.00372.x.
- KRAUSE, S., LIEBETRAU, V., GORB, S., SÁNCHEZ-ROMÁN, M., MCKENZIE, J.A., AND TREUDE, T., 2012, Microbial nucleation of Mg-rich dolomite in exopolymeric substances under anoxic modern seawater salinity: new insight into an old enigma: *Geology*, v. 40, p. 587–590, doi: 10.1130/G32923.1.
- KRAUSKOPF, K.B., 1956, Dissolution and precipitation of silica at low temperatures: *Geochimica et Cosmochimica Acta*, v. 10, p. 1–26, doi: 10.1016/0016-7037(56)90009-6.
- LAI, V.M.F., WONG, P.A.-L., AND LI, C.-Y., 2000, Effects of cation properties on sol-gel transition and gel properties of κ-carrageenan: *Journal of Food Science*, v. 65, p. 1332–1337, doi: 10.1111/j.1365-2621.2000.tb10607.x.
- LEE, J.-B., HAYASHI, T., HAYASHI, K., SANKAWA, U., MAEDA, M., NEMOTO, T., AND NAKANISHI, H., 1998, Further purification and structural analysis of calcium spirulin from *Spirulina platensis*: *Journal of Natural Products*, v. 61, p. 1101–1104, doi: 10.1021/np980143n.
- LEO, R.F. AND BARGHOORN, E.S., 1976, Silicification of wood: *Botanical Museum Leaflets, Harvard University*, v. 25, p. 1–47.
- LUDWIG, R., AL-HORANI, F.A., DE BEER, D., AND JONKERS, H.M., 2005, Photosynthesis-controlled calcification in a hypersaline microbial mat: *Limnology and Oceanography*, v. 50, p. 1836–1843, doi: 10.4319/lo.2005.50.6.1836.
- MALIVA, R.G., KNOLL, A.H., AND SIEVER, R., 1989, Secular change in chert distribution; a reflection of evolving biological participation in the silica cycle: *PALAIOS*, v. 4, p. 519–532, doi: 10.2307/3514743.
- MANNING-BERG, A.R. AND KAH, L.C., 2017, Proterozoic microbial mats and their constraints on environments of silicification: *Geobiology*, v. 15, p. 469–483, doi: 10.1111/gbi.12238.
- MICHALOPOULOS, P. AND ALLER, R.C., 2004, Early diagenesis of biogenic silica in the Amazon delta: alteration, authigenic clay formation, and storage: *Geochimica et Cosmochimica Acta*, v. 68, p. 1061–1085, doi: 10.1016/j.gca.2003.07.018.
- MOORE, K.R., BOSAK, T., MACDONALD, F.A., DU, K., NEWMAN, S., LAHR, D.J.G., AND PRUSS, S.B., 2017a, Pyritized cryogenian cyanobacterial fossils from Arctic Alaska: *PALAIOS*, v. 32, p. 769–778, doi: 10.2110/palo.2017.063.
- MOORE, K.R., BOSAK, T., MACDONALD, F.A., LAHR, D.J.G., NEWMAN, S., SETTENS, C., AND PRUSS, S.B., 2017b, Biologically agglutinated eukaryotic microfossil from Cryogenian cap carbonates: *Geobiology*, v. 15, p. 499–515, doi: 10.1111/gbi.12225.
- MOORE, K.R., GONG, J., PAJUSALU, M., SKOOG, E.J., XU, M., FELIZ SOTO, T., SOJO, V., MATREUX, T., BALDES, M.J., BRAUN, D., WILLIFORD, K., AND BOSAK, T., 2021, A new model for silicification of cyanobacteria in Proterozoic tidal flats: *Geobiology*, v. 19, p. 438–449, doi: 10.1111/gbi.12447.
- MOORE, K.R., PAJUSALU, M., GONG, J., SOJO, V., MATREUX, T., BRAUN, D., AND BOSAK, T., 2020, Biologically mediated silicification of marine cyanobacteria and implications for the Proterozoic fossil record: *Geology*, v. 48, p. 862–866, doi: 10.1130/G47394.1.
- MYSEN, B.O., FINGER, L.W., VIRGO, D., AND SEIFERT, F.A., 1982, Curve-fitting of Raman spectra of silicate glasses: *American Mineralogist*, v. 67, p. 686–695.
- NEWMAN, S.A., KLEPAC-CERAJ, V., MARIOTTI, G., PRUSS, S.B., WATSON, N., AND BOSAK, T., 2017, Experimental fossilization of mat-forming cyanobacteria in coarse-grained siliclastic sediments: *Geobiology*, v. 15, p. 484–498, doi: 10.1111/gbi.12229.
- NEWMAN, S.A., MARIOTTI, G., PRUSS, S., AND BOSAK, T., 2016, Insights into cyanobacterial fossilization in Ediacaran siliclastic environments: *Geology*, v. 44, p. 579–582, doi: 10.1130/G37791.1.
- OEHLER, D.Z., 1978, Microflora of the middle Proterozoic Balbirini Dolomite (McArthur Group) of Australia: *Alcheringa: An Australasian Journal of Palaeontology*, v. 2, p. 269–309, doi: 10.1080/03115517808527785.
- ORANGE, F., LALONDE, S.V., AND KONHAUSER, K.O., 2013, Experimental simulation of evaporation-driven silica sinter formation and microbial silicification in hot spring systems: *Astrobiology*, v. 13, p. 163–176, doi: 10.1089/ast.2012.0887.
- OUIWERX, C., VELINGS, N., MESTDAGH, M.M., AND AXELOS, M.A.V., 1998, Physico-chemical properties and rheology of alginate gel beads formed with various divalent cations: *Polymer Gels and Networks*, v. 6, p. 393–408, doi: 10.1016/S0966-7822(98)00035-5.
- OWEN, L.B., 1975, Precipitation of amorphous silica from high-temperature hypersaline geothermal brines: Lawrence Livermore Laboratory Report, number UCRL-51866, 24 p.
- PAGE, R.W., JACKSON, M.J., AND KRASSAY, A.A., 2000, Constraining sequence stratigraphy in north Australian basins: SHRIMP U–Pb zircon geochronology between Mt Isa and McArthur River: *Australian Journal of Earth Sciences*, v. 47, p. 431–459, doi: 10.1046/j.1440-0952.2000.00797.x.
- PARKHURST, D.L. AND APPELO, C.A.J., 2013, Description of input and examples for PHREEQC version 3: a computer program for speciation, batch-reaction, one-dimensional transport, and inverse geochemical calculations: U.S. Geological Survey Techniques and Methods USGS Numbered Series 6-A43, 519 p., <http://pubs.er.usgs.gov/publication/tm6A43>. Checked January 2022.
- PERRI, E., TUCKER, M.E., SŁOWAKIEWICZ, M., WHITAKER, F., BOWEN, L., AND PERROTTA, I.D., 2018, Carbonate and silicate biomineralization in a hypersaline microbial mat (Mesaieed sabkha, Qatar): roles of bacteria, extracellular polymeric substances and viruses: *Sedimentology*, v. 65, p. 1213–1245, doi: 10.1111/sed.12419.
- RAZZELL HOLLIS, J., IRELAND, S., ABBEY, W., BHARTIA, R., AND BEEGLE, L.W., 2021, Deep-ultraviolet Raman spectra of Mars-relevant evaporite minerals under 248.6 nm excitation: *Icarus*, v. 357, article 114067, doi: 10.1016/j.icarus.2020.114067.
- RENAUT, R.W., JONES, B., AND TIERCELIN, J.-J., 1998, Rapid in situ silicification of microbes at Loburu hot springs, Lake Bogoria, Kenya Rift Valley: *Sedimentology*, v. 45, p. 1083–1103, doi: 10.1046/j.1365-3091.1998.00194.x.
- RIDING, R., (ed.), 1991, *Calcareous Algae and Stromatolites*: Springer-Verlag Berlin Heidelberg, 334 p.
- RIDING, R., 1982, Cyanophyte calcification and changes in ocean chemistry: *Nature*, v. 299, p. 814–815, doi: 10.1038/299814a0.
- ROBERTS, J.A., KENWARD, P.A., FOWLE, D.A., GOLDSTEIN, R.H., GONZÁLEZ, L.A., AND MOORE, D.S., 2013, Surface chemistry allows for abiotic precipitation of dolomite at low temperature: *Proceedings of the National Academy of Sciences*, v. 110, p. 14540–14545, doi: 10.1073/pnas.1305403110.
- RODGERS, K.A., BROWNE, P.R.L., BUDDLE, T.F., COOK, K.L., GREATREX, R.A., HAMPTON, W.A., HERDIANTA, N.R., HOLLAND, G.R., LYNNE, B.Y., MARTIN, R., NEWTON, Z., PASTARS, D., SANNAZZARRO, K.L., AND TEECE, C.I.A., 2004, Silica phases in sinters and residues from geothermal fields of New Zealand: *Earth-Science Reviews*, v. 66, p. 1–61, doi: 10.1016/j.earscirev.2003.10.001.
- SCHOPE, J.W. AND KLEIN, C., 1992, *The Proterozoic Biosphere: A Multidisciplinary Study*: Cambridge University Press, Cambridge, UK, 1408 p.
- SCHOPE, J.W., KUDRYAVTSEV, A.B., WALTER, M.R., VAN KRANENDONK, M.J., WILLIFORD, K.H., KOZDON, R., VALLEY, J.W., GALLARDO, V.A., ESPINOZA, C., AND FLANNERY, D.T., 2015, Sulfur-cycling fossil bacteria from the 1.8-Ga Duck Creek Formation provide promising evidence of evolution's null hypothesis: *Proceedings of the National Academy of Sciences*, v. 112, p. 2087–2092, doi: 10.1073/pnas.1419241112.
- SCHULTZE-LAM, S., FERRIS, F.G., KONHAUSER, K.O., AND WIESE, R.G., 1995, In situ silicification of an Icelandic hot spring microbial mat: implications for microfossil formation: *Canadian Journal of Earth Sciences*, v. 32, p. 2021–2026, doi: 10.1139/e95-155.
- SCHULTZE-LAM, S., THOMPSON, J.B., AND BEVERIDGE, T.J., 1993, Metal ion immobilization by bacterial surfaces in freshwater environments: *Water Quality Research Journal*, v. 28, p. 51–82, doi: 10.2166/wqrj.1993.004.
- SERGEEV, V.N., KNOLL, A.H., AND GROTZINGER, J.P., 1995, Paleobiology of the Mesoproterozoic Bilyakh Group, Anabar Uplift, Northern Siberia: *Memoir of the Paleontological Society*, v. 39, p. 1–37.
- SERGEEV, V.N., KNOLL, A.H., AND PETROV, P.Y.U., 1997, Paleobiology of the Mesoproterozoic–Neoproterozoic transition: the Sukhaya Tunguska Formation, Turukhansk Uplift, Siberia: *Precambrian Research*, v. 85, p. 201–239, doi: 10.1016/S0301-9268(97)00035-1.
- SERGEEV, V.N. AND SHARMA, M., 2012, Proterozoic fossil cyanobacteria: *Palaeobotanist*, v. 61, p. 189–358.

- SHI, M., FENG, Q., KHAN, M.Z., AND ZHU, S., 2017, An eukaryote-bearing microbiota from the Early Mesoproterozoic Gaoyuzhuang Formation, Tianjin, China and its significance: *Precambrian Research*, v. 303, p. 709–726, doi: 10.1016/j.precamres.2017.09.013.
- SHIMADA, K. AND TARUTANI, T., 1980, The kinetics of the polymerization of silicic acid: *Bulletin of the Chemical Society of Japan*, v. 53, p. 3488–3491.
- SIEVER, R., 1992, The silica cycle in the Precambrian: *Geochimica et Cosmochimica Acta*, v. 56, p. 3265–3272, doi: 10.1016/0016-7037(92)90303-Z.
- SOUZA-EGIPSY, V., WIERZCHOS, J., ASCASO, C., AND NEALSON, K.H., 2005, Mg-silica precipitation in fossilization mechanisms of sand tufa endolithic microbial community, Mono Lake (California): *Chemical Geology*, v. 217, p. 77–87, doi: 10.1016/j.chemgeo.2004.12.004.
- STANEVICH, A.M., MAKSIMOVA, E.N., KORNILOVA, T.A., GLADKOCHUB, D.P., MAZUKABZOV, A.M., AND DONSKAYA, T.V., 2009, Microfossils from the Arymas and Debengda formations, the Riphean of the Olenek Uplift: age and presumable nature: *Stratigraphy and Geological Correlation*, v. 17, p. 20–35, doi: 10.1134/S086959380901002X.
- STRICKLAND, J.D.H. AND PARSONS, T.R., 1972, Determination of reactive silicate, in *A Practical Handbook of Seawater Analysis: Fisheries Research Board of Canada*, Ottawa, p. 65–70.
- TOSCA, N.J., MACDONALD, F.A., STRAUSS, J.V., JOHNSTON, D.T., AND KNOLL, A.H., 2011, Sedimentary talc in Neoproterozoic carbonate successions: *Earth and Planetary Science Letters*, v. 306, p. 11–22, doi: 10.1016/j.epsl.2011.03.041.
- TRÉGUER, P., NELSON, D.M., VAN BENNEKOM, A.J., DEMASTER, D.J., LEYNAERT, A., AND QUÉGUINER, B., 1995, The silica balance in the world ocean: a reestimate: *Science*, v. 268, p. 375–379.
- TYLER, S.A. AND BARGHOORN, E.S., 1954, Occurrence of structurally preserved plants in Pre-Cambrian rocks of the Canadian Shield: *Science*, v. 119, p. 606–608, doi: 10.1126/science.119.3096.606.
- URRUTIA, M.M. AND BEVERIDGE, T.J., 1993, Remobilization of heavy metals retained as oxyhydroxides or silicates by *Bacillus subtilis* cells: *Applied and Environmental Microbiology*, v. 59, p. 4323–4329.
- URRUTIA, M.M. AND BEVERIDGE, T.J., 1994, Formation of fine-grained metal and silicate precipitates on a bacterial surface (*Bacillus subtilis*): *Chemical Geology*, v. 116, p. 261–280, doi: 10.1016/0009-2541(94)90018-3.
- VAN LITH, Y., WARTHMAN, R., VASCONCELOS, C., AND MCKENZIE, J.A., 2003, Sulphate-reducing bacteria induce low-temperature Ca-dolomite and high Mg-calcite formation: *Geobiology*, v. 1, p. 71–79, doi: 10.1046/j.1472-4669.2003.00003.x.
- VOROB'ÉVA, N.G., SERGEEV, V.N., AND PETROV, P.YU. 2015, Kotuikan Formation assemblage: a diverse organic-walled microbiota in the Mesoproterozoic Anabar succession, northern Siberia: *Precambrian Research*, v. 256, p. 201–222.
- WILMETH, D.T., MYERS, K.D., LALONDE, S.V., MÄND, K., KONHAUSER, K.O., GRANDIN, P., AND VAN ZUILEN, M.A., 2021, Evaporative silicification in floating microbial mats: patterns of oxygen production and preservation potential in silica-undersaturated streams, El Tatio, Chile: *Geobiology*, v. 20, p. 1–21, doi: 10.1111/gbi.12476.
- WILSON, J.P., FISCHER, W.W., JOHNSTON, D.T., KNOLL, A.H., GROTZINGER, J.P., WALTER, M.R., MCNAUGHTON, N.J., SIMON, M., ABELSON, J., SCHRAG, D.P., SUMMONS, R., ALLWOOD, A., ANDRES, M., GAMMON, C., ET AL., 2010, Geobiology of the late Paleoproterozoic Duck Creek Formation, Western Australia: *Precambrian Research*, v. 179, p. 135–149, doi: 10.1016/j.precamres.2010.02.019.

Received 28 February 2022; accepted 28 June 2022.